

# Preparation of a $\text{H}_3\text{PW}_{12}\text{O}_{40}$ Deposited Chitosan Coated Iron Oxide Magnetic Core–Shell Nanocomposite for Friedel-Crafts Acylation

Xin Wen, Huanhuan Zhang, Fei Tian, Xiaofang Liu, Libo Niu, and Guoyi Bai\*

*Key Laboratory of Chemical Biology of Hebei Province, College of Chemistry and Environmental Science, Hebei University, Baoding, Hebei, 071002, China*

A novel  $\text{H}_3\text{PW}_{12}\text{O}_{40}$  deposited chitosan coated iron oxide magnetic core–shell nanocomposite ( $\text{Fe}_3\text{O}_4@CS@HPW$ ) was prepared via a facile approach.  $\text{Fe}_3\text{O}_4$  nanoparticles were first coated with crosslinking-agent-free chitosan, and then  $\text{H}_3\text{PW}_{12}\text{O}_{40}$  was loaded onto the surface of chitosan as an outer shell. The resultant nanocomposite was well characterized by Brunauer-Emmett-Teller surface area analysis (BET), inductively coupled plasma analysis (ICP), X-ray diffraction (XRD), fourier transform infrared spectroscopy (FTIR), transmission electron microscopy (TEM) and elemental mappings.  $\text{Fe}_3\text{O}_4@CS@HPW$  showed better catalytic performance than its counterpart with a chitosan-crosslinked shell in the Friedel-Crafts acylation of anisole to 4-methoxyacetophenone under solvent-free conditions, and can be easily separated by an external magnetic field and recycled effectively.

**Keywords:** Magnetic, Chitosan, Composite Materials,  $\text{H}_3\text{PW}_{12}\text{O}_{40}$ , Catalysis.

## 1. INTRODUCTION

Solid acids, especially  $\text{H}_3\text{PW}_{12}\text{O}_{40}$  (HPW), are believed as an important class of catalysts in a number of chemical processes,<sup>1–3</sup> such as Friedel-Crafts acylation,<sup>4</sup> esterification,<sup>5</sup> oxidation<sup>6,7</sup> and the biodiesel production,<sup>8</sup> due to the low corrosivity, low volatility, high activity and strong acidity. However, the major problems in applying HPW are its poor solubility in polar media, poor hydrothermal stability and low surface area. Therefore, various nanomaterials, such as molecular sieve<sup>9</sup> and mesoporous silica,<sup>10</sup> are applied as catalyst supports to overcome these shortcomings. For example, Brahmkhatri et al.<sup>10</sup> have prepared a SBA-15 anchored HPW catalyst, which showed an excellent activity in biodiesel production by esterification of free fatty acid.

As is well known, magnetic separation provides a quick, simple, eco-friendly, and effective method for removing and recycling magnetic particles. Some inorganic materials, including silica and carbon, have been applied as a shell to coat the magnetic cores.<sup>11–15</sup> Recently, natural materials, particularly chitosan (CS), have proven

to be a kind of promising coating materials to prepare magnetic core–shell materials due to their special structural properties and environmentally benign nature.<sup>16–21</sup> For instance, magnetically recoverable  $\text{Fe}_3\text{O}_4@CS$  prepared by a crosslinking-process has been used as a carrier to immobilize protonated peroxotungstate and the obtained core–shell nanocomposite exhibited high catalytic activity and stability in catalytic oxidation.<sup>18</sup> However, surface modification of  $\text{Fe}_3\text{O}_4$  and addition of crosslinking agent are generally necessary to form a chitosan shell on the surface of  $\text{Fe}_3\text{O}_4$  during the preparation of magnetic core–shell materials, making the preparation processes complex and environmentally unfriendly.<sup>21–25</sup> Thus, there is still a need to develop a facile and green method to prepare chitosan coated magnetic core–shell materials.

In continuation of our previous work,<sup>4,13</sup> we herein report the construction of a novel  $\text{H}_3\text{PW}_{12}\text{O}_{40}$  deposited chitosan coated iron oxide magnetic core–shell nanocomposite ( $\text{Fe}_3\text{O}_4@CS@HPW$ ) without addition of any crosslinking agent. The obtained  $\text{Fe}_3\text{O}_4@CS@HPW$  nanocomposite showed good catalytic performance in the Friedel-Crafts acylation of anisole to 4-methoxyacetophenone under solvent-free conditions. Furthermore,

\*Author to whom correspondence should be addressed.

it can be easily separated due to its high saturation magnetization and recycled effectively.

## 2. EXPERIMENTAL DETAILS

### 2.1. Preparation of Magnetic Core–Shell Nanocomposites

Unless otherwise noted, all chemicals were of analytical reagent grade and used without further purification. Fe<sub>3</sub>O<sub>4</sub>@CS@HPW was prepared by the following procedure. In brief, CS (0.3 g) was dissolved in acetic acid solution (0.05 M, 130 mL) under stirring for 30 min, followed by adding Fe<sub>3</sub>O<sub>4</sub> nanoparticles (0.75 g). Aqueous solution of NaOH (1.25 M, 8 mL) was then slowly added and stirred for another 30 min at room temperature. After separated by a magnet, the Fe<sub>3</sub>O<sub>4</sub>@CS so obtained was washed with water and ethanol, and then 60 mL aqueous solution containing HPW (2.0 g) was added, followed by stirring for 2 h. Finally, Fe<sub>3</sub>O<sub>4</sub>@CS@HPW was collected by a magnet, heated at 250 °C for 4 h. When HPW was not used, the product was denoted as Fe<sub>3</sub>O<sub>4</sub>@CS.

The nanocomposite with a chitosan-crosslinked shell was prepared by the following procedure and denoted as Fe<sub>3</sub>O<sub>4</sub>@cl-CS@HPW. CS (0.3 g) was dissolved in acetic acid solution (0.05 M, 130 mL) under stirring for 30 min, followed by adding Fe<sub>3</sub>O<sub>4</sub> nanoparticles (0.75 g). Subsequently, 3 mL of aqueous solution containing 1,5-pentanedial (0.115 g) was added, followed by stirring at 60 °C for 2 h. Then, HPW (2.0 g) was added to the resulting mixture and stirred for 2 h. Finally, the product was collected by a magnet, heated at 250 °C for 4 h.

When Fe<sub>3</sub>O<sub>4</sub> was directly used as the support of HPW, the nanocomposite was prepared by the following procedure and denoted as Fe<sub>3</sub>O<sub>4</sub>@HPW. To 25 mL of aqueous solution containing HPW (0.6 g), 1.4 g of Fe<sub>3</sub>O<sub>4</sub> nanoparticles was added and stirred for 4 h at room temperature. Finally, the product was collected by a magnet, heated at 250 °C for 4 h.

### 2.2. Characterization

Brunauer-Emmett-Teller (BET) surface area was estimated on a Micromeritics Tristar II 3020 surface area and pore analyzer. X-ray diffraction (XRD) patterns were collected on a Bruker D8-ADVANCE X-ray diffractometer using Cu K $\alpha$  radiation and a scan step of 0.02° at 20 °C. Transmission electron microscopy (TEM) images were obtained with a FEI Tecnai G2 F20 S-Twin instrument at a voltage of 200 kV. Fourier transform infrared spectroscopy (FTIR) was carried out on a Bruker Vertex 70 spectrophotometer (KBr pellet technique). Inductively coupled plasma analysis (ICP) was measured on a Varian Vista-MPX spectrometer. Magnetization curves were obtained on a LDJ9600-1 Superconducting quantum interference device.

### 2.3. Activity Test

To a round-bottom flask equipped with a water condenser, acetic anhydride (0.54 g, 5 mmol), anisole (1.08 g, 10 mmol) and nanocomposite (0.15 g) were added and the reaction mixture was stirred at 154 °C for 4 h. When the reaction was completed, the reaction mixture was allowed to cool to room temperature and separated using a permanent magnet. The products were analyzed by gas chromatography using a 30-m SE-54 capillary column, and their structures were identified by gas chromatography–mass spectroscopy (GC-MS) on a Thermo Finnigan Polaris-Q spectrometer.

## 3. RESULTS AND DISCUSSION

Textural properties of the magnetic core–shell nanocomposites are summarized in Table I. It was found that Fe<sub>3</sub>O<sub>4</sub>@CS exhibited the highest surface area and pore volume in the nanocomposites studied. The surface area and pore volume of Fe<sub>3</sub>O<sub>4</sub>@CS@HPW and Fe<sub>3</sub>O<sub>4</sub>@cl-CS@HPW decreased markedly after the loading of HPW, which could be attributed to the occupation of HPW on the surface and in the pores of the chitosan shell.<sup>26</sup> With respect to tungsten content, both Fe<sub>3</sub>O<sub>4</sub>@CS@HPW and Fe<sub>3</sub>O<sub>4</sub>@cl-CS@HPW possessed more tungsten element compared with Fe<sub>3</sub>O<sub>4</sub>@HPW, which could be ascribed to abundant complexation sites on the chitosan shell, suggesting the positive effect of chitosan shell on HPW loading. Moreover, Fe<sub>3</sub>O<sub>4</sub>@CS@HPW had a larger content of tungsten element than Fe<sub>3</sub>O<sub>4</sub>@cl-CS@HPW, probably due to the consumption of complexation sites for HPW during the crosslinking process.

Figure 1 shows XRD patterns of the nanocomposites. Compared curves d and e with a, the diffraction peaks of HPW became broader and weaker in the chitosan coated nanocomposites, indicating that the HPW was highly dispersed on the chitosan shell with an amorphous structure.<sup>27</sup> Furthermore, the characteristic diffractions of the Fe<sub>3</sub>O<sub>4</sub>-contained nanocomposites (curves b, c, d and e) showed peaks at 30.1°, 35.4°, 43.1°, 53.8°, 57.0° and 62.5°, which could be assigned to Fe<sub>3</sub>O<sub>4</sub> cores,<sup>28</sup> suggesting that Fe<sub>3</sub>O<sub>4</sub> cores retained their magnetite crystalline structures after the addition of HPW.

In the FTIR spectrum of Fe<sub>3</sub>O<sub>4</sub>@CS, the characteristic peaks of chitosan (mainly at 3440, 2880, 1649, 1596, 1384, and 1079 cm<sup>-1</sup>) were weakened markedly

**Table I.** Textural properties of the core–shell nanocomposites.

Nanocomposite	Tungsten content <sup>a</sup> (%)	Surface area (m <sup>2</sup> /g)	Pore volume (cm <sup>3</sup> /g)
Fe <sub>3</sub> O <sub>4</sub> @CS	–	10.0	0.022
Fe <sub>3</sub> O <sub>4</sub> @cl-CS@HPW	36.1	1.7	0.007
Fe <sub>3</sub> O <sub>4</sub> @CS@HPW	41.2	2.1	0.007
Fe <sub>3</sub> O <sub>4</sub> @HPW	1.1	4.0	0.011

Notes: <sup>a</sup>Based on ICP results.

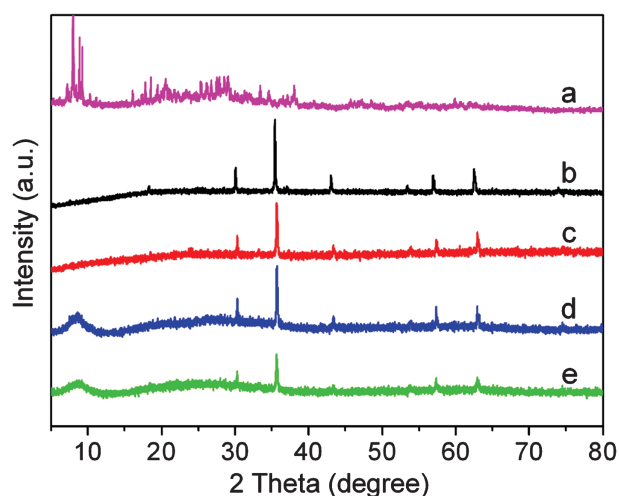


**Figure 1.** XRD patterns of (a) HPW, (b)  $\text{Fe}_3\text{O}_4$ , (c)  $\text{Fe}_3\text{O}_4@CS$ , (d)  $\text{Fe}_3\text{O}_4@CS@HPW$  and (e)  $\text{Fe}_3\text{O}_4@cl-CS@HPW$ .

compared with the pure chitosan (Figs. 2, curves a and b),<sup>29</sup> probably due to the low content of chitosan. After the loading of HPW, these peaks were further weakened in  $\text{Fe}_3\text{O}_4@CS@HPW$  and  $\text{Fe}_3\text{O}_4@cl-CS@HPW$  (Figs. 2, curves d and e), however, the characteristic peaks of HPW appeared at 1081, 982, 889, 797 and 595  $\text{cm}^{-1}$  (Fig. 2, curve c), indicating the existence of HPW in  $\text{Fe}_3\text{O}_4@CS@HPW$  and  $\text{Fe}_3\text{O}_4@cl-CS@HPW$ .

TEM images and the related elemental mapping of  $\text{Fe}_3\text{O}_4@CS@HPW$  are shown in Figure 3. It was obvious that the  $\text{Fe}_3\text{O}_4$  cores were coated with a chitosan shell and the particle sizes of these nanocomposites were roughly 200 nm (Figs. 2(a–c)). It is difficult to confirm the existence of HPW on the surface of  $\text{Fe}_3\text{O}_4@CS$  only from the TEM images, which was mainly ascribed to the highly dispersed and poorly crystallized HPW species. However, the existence of HPW and the core–shell

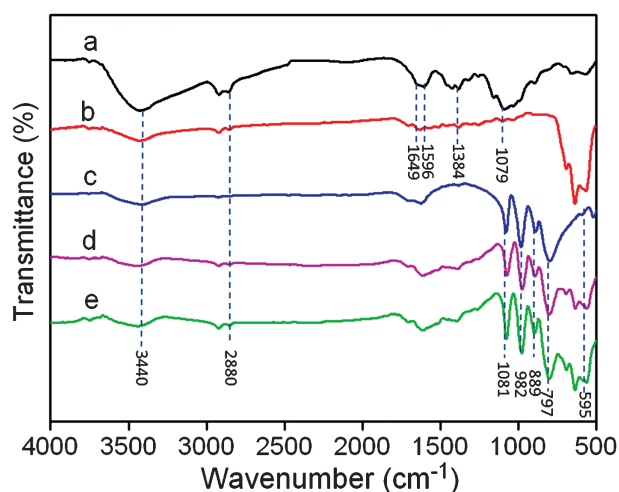


**Figure 2.** FT-IR spectra of (a) CS, (b)  $\text{Fe}_3\text{O}_4@CS$ , (c) HPW, (d)  $\text{Fe}_3\text{O}_4@CS@HPW$  and (e)  $\text{Fe}_3\text{O}_4@cl-CS@HPW$ .

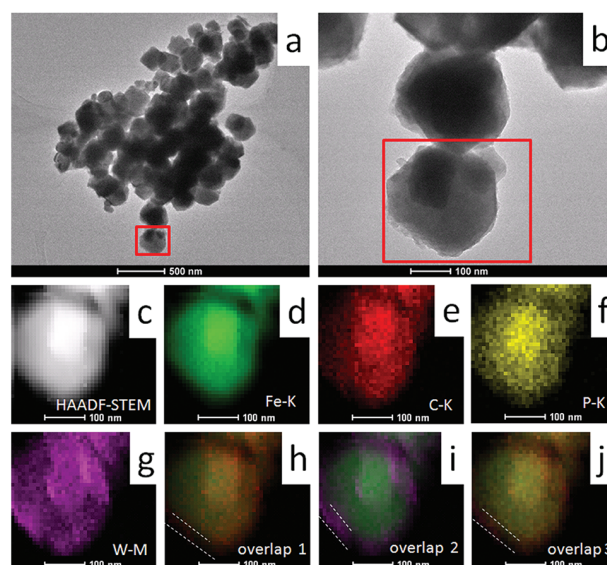


**Figure 3.** TEM images of  $\text{Fe}_3\text{O}_4@CS@HPW$  (a and b); HAADF-STEM image of  $\text{Fe}_3\text{O}_4@CS@HPW$  (c), with elemental mappings of (d) Fe, (e) C, (f) P, (g) W, (h) the overlap of Fe and C, (i) the overlap of Fe and W, and (j) the overlap of Fe, C, P and W.

structure of  $\text{Fe}_3\text{O}_4@CS@HPW$  were convincingly proved by the elements mappings of the related Fe, C, P, W, and their overlaps (Figs. 2(d–j)). Furthermore,  $\text{Fe}_3\text{O}_4@cl-CS@HPW$  exhibited a similar particle sizes and morphology to  $\text{Fe}_3\text{O}_4@CS@HPW$  (not shown).

The room-temperature hysteresis loops of the nanocomposites are shown in Figure 4. The saturation magnetization ( $M_s$ ) value of  $\text{Fe}_3\text{O}_4@CS@HPW$  and  $\text{Fe}_3\text{O}_4@cl-CS@HPW$  were 13.2 emu/g and 17.1 emu/g at an applied field of 60 000 Oe, respectively. No remanence or hysteresis loops were detected, indicating their super-paramagnetism.<sup>30</sup> In addition, the  $M_s$  values of  $\text{Fe}_3\text{O}_4@CS@HPW$  and  $\text{Fe}_3\text{O}_4@cl-CS@HPW$  decreased markedly compared with  $\text{Fe}_3\text{O}_4$ , probably due to the cladding of chitosan and HPW on the surface of  $\text{Fe}_3\text{O}_4$ . Nevertheless,  $\text{Fe}_3\text{O}_4@CS@HPW$  could still be easily separated within 12 seconds by a permanent magnet (the inset of Fig. 4).

The catalytic performance of  $\text{Fe}_3\text{O}_4@CS@HPW$ ,  $\text{Fe}_3\text{O}_4@cl-CS@HPW$  and  $\text{Fe}_3\text{O}_4@HPW$  were tested in the Friedel-Crafts acylation of anisole with acetic anhydride under solvent-free conditions and the results are listed in Table II. As can be seen,  $\text{Fe}_3\text{O}_4@HPW$  showed a terribly low conversion (6.6%). With the introduction of chitosan-crosslinked shell,  $\text{Fe}_3\text{O}_4@cl-CS@HPW$  exhibited a much better catalytic activity (76.2%), which was attributed to the increasing content of HPW, showing the necessity of chitosan shell in the core–shell nanocomposites. Particularly, when the crosslinking agent was not used in the preparation process,  $\text{Fe}_3\text{O}_4@CS@HPW$  showed the best conversion of acetic anhydride (94.1%), with a selectivity for 4-methoxyacetophenone of 94.8%, which was higher than that of  $\text{Fe}_3\text{O}_4@cl-CS@HPW$ . These results can

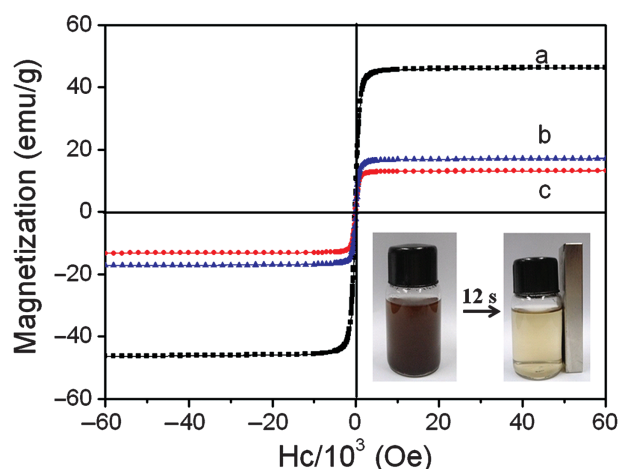


**Figure 4.** Room temperature hysteresis loops of (a)  $\text{Fe}_3\text{O}_4$ , (b)  $\text{Fe}_3\text{O}_4$ @cl-CS@HPW and (c)  $\text{Fe}_3\text{O}_4$ @CS@HPW. The inset is a photograph of  $\text{Fe}_3\text{O}_4$ @CS@HPW before and after magnetic separation by an external magnetic field.

be explained by the consumption of some complexation sites during the crosslinking process and in turn its lower HPW content, as demonstrated by ICP result, accounting for the lower activity of  $\text{Fe}_3\text{O}_4$ @cl-CS@HPW. Thus, a crosslinking-agent-free chitosan shell is proven to be crucial for the effective assembling of HPW on the surface of  $\text{Fe}_3\text{O}_4$ .

The easy separation and reusability are the main advantages of magnetic catalysts. Therefore, we investigated the stability of the  $\text{Fe}_3\text{O}_4$ @CS@HPW catalyst in repeated cycles of reaction. At the end of the first cycle,  $\text{Fe}_3\text{O}_4$ @CS@HPW could be easily separated from the reaction mixture using a permanent magnet. Then the catalyst was washed thoroughly with acetone, heated at 250 °C for 4 h and reused for the next cycle of reaction under the same conditions. As presented in Figure 5,  $\text{Fe}_3\text{O}_4$ @CS@HPW kept stable and exhibited a high catalytic activity within four cycles. The good reusability rendered us to believe that  $\text{Fe}_3\text{O}_4$ @CS@HPW was a promising catalyst for Friedel-Crafts acylation under solvent-free conditions.

**Table II.** Catalytic performance of HPW catalysts in the Friedel-Crafts acylation.<sup>a</sup>

Nanocomposite	Conversion (%)	Selectivity (%)	Yield (%)
$\text{Fe}_3\text{O}_4$ @HPW	6.6	88.5	5.8
$\text{Fe}_3\text{O}_4$ @cl-CS@HPW	76.2	94.4	71.9
$\text{Fe}_3\text{O}_4$ @CS@HPW	94.1	94.8	89.2

Notes: <sup>a</sup>Reaction conditions: Acetic anhydride (5 mmol), anisole (10 mmol) and nanocomposite (0.15 g), temperature at 154 °C and reaction time 4 h.

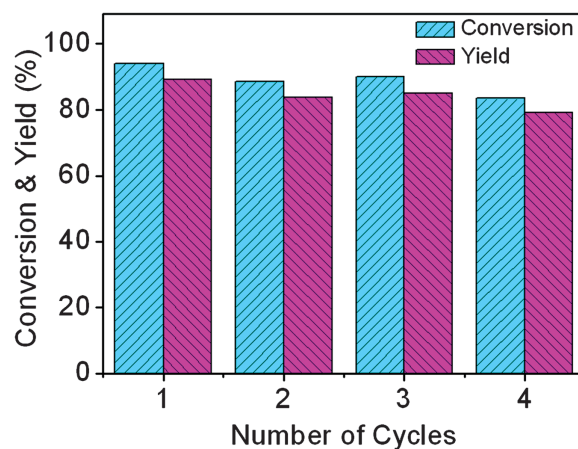


**Figure 5.** Reusability of  $\text{Fe}_3\text{O}_4$ @CS@HPW in the Friedel-Crafts acylation of anisole with acetic anhydride under solvent-free conditions.

#### 4. CONCLUSIONS

In summary, a novel  $\text{Fe}_3\text{O}_4$ @CS@HPW magnetic core-shell nanocomposite has been successfully prepared via a green and facile approach. Structural characterizations demonstrated that the as-prepared core-shell nanocomposite was composed of a  $\text{Fe}_3\text{O}_4$  core, a chitosan shell and a HPW outer shell. This nanocomposite showed high activity and good selectivity in the Friedel-Crafts acylation of anisole under solvent-free conditions, superior to  $\text{Fe}_3\text{O}_4$ @cl-CS@HPW with a chitosan-crosslinked shell. Moreover, it can be easily separated and reused after reaction due to its high saturation magnetization.

**Acknowledgments:** Financial support by the National Natural Science Foundation of China (21376060) and the Natural Science Foundation of Hebei Province (B2014201024 and B2016418005) is gratefully acknowledged.

#### References and Notes

- K. Inumaru, T. Ishihara, Y. Kamiya, T. Okuhara, and S. Yamanaka, *Angew. Chem. Int. Ed.* 46, 7625 (2007).
- J. K. Kim, H. W. Park, U. G. Hong, J. H. Choi, and I. K. Song, *J. Nanosci. Nanotechnol.* 14, 8884 (2014).
- D. Nedumaran and A. Pandurangan, *J. Nanosci. Nanotechnol.* 14, 2799 (2014).
- G. Bai, T. Li, Y. Yang, H. Zhang, X. Lan, F. Li, J. Han, Z. Ma, Q. Chen, and G. Chen, *Catal. Commun.* 29, 114 (2012).
- S. Li, S. R. Zhai, J. M. Zhang, Z. Y. Xiao, Q. D. An, M. H. Li, and X. W. Song, *Eur. J. Inorg. Chem.* 31, 5428 (2013).
- X. Cai, H. Wang, Q. Zhang, J. Tong, and Z. Lei, *J. Mol. Catal. A* 383–384, 217 (2014).
- T. V. Rao, K. Haribabu, P. S. S. Prasad, and N. Lingaiah, *Green Chem.* 15, 837 (2013).
- C. Baroi and A. K. Dalai, *Ind. Eng. Chem. Res.* 53, 18611 (2014).
- A. Patel and N. Narkhede, *Energ. Fuel* 26, 6025 (2012).
- V. Brahmkhatri and A. Patel, *Appl. Catal. A* 403, 161 (2011).
- D. Wang and D. Astruc, *Chem. Rev.* 114, 6949 (2014).
- G. Bai, X. Lan, X. Liu, C. Liu, L. Shi, Q. Chen, and G. Chen, *Green Chem.* 16, 3160 (2014).

13. G. Bai, L. Shi, Z. Zhao, Y. Wang, M. Qiu, and H. Dong, *Mater. Lett.* 96, 93 (2013).
14. M. Shokouhimehr, K. Y. Shin, J. S. Lee, M. J. Hackett, S. W. Jun, M. H. Oh, J. Jang, and T. Hyeon, *J. Mater. Chem. A* 2, 7593 (2014).
15. P. Shen, H. Zhang, H. Liu, J. Y. Xin, L. F. Fei, X. G. Luo, and S. J. Zhang, *J. Mater. Chem. A* 3, 3456 (2015).
16. Y. Qiu, Z. Ma, and P. Hu, *J. Mater. Chem. A* 2, 13471 (2014).
17. A. Kong, P. Wang, H. Zhang, F. Yang, S. Huang, and Y. Shan, *Appl. Catal. A* 417–418, 183 (2012).
18. J. Zhu, P. C. Wang, and M. Lu, *New J. Chem.* 36, 2587 (2012).
19. Y. Zhan, X. Tan, G. Lai, A. Yu, D. Han, and H. Zhang, *Nanosci. Nanotechnol. Lett.* 5, 684 (2013).
20. S. Peng, H. C. Meng, L. Zhou, and J. Chang, *J. Nanosci. Nanotechnol.* 14, 7010 (2014).
21. A. L. Kavitha, H. G. Prabu, S. A. Babu, and S. K. Suja, *J. Nanosci. Nanotechnol.* 13, 98 (2013).
22. L. He, L. Yao, F. Liu, B. Qin, R. Song, and W. Huang, *J. Nanosci. Nanotechnol.* 10, 6348 (2010).
23. A. Maleki, N. Ghamari, and M. Kamalzare, *RSC Adv.* 4, 9416 (2014).
24. G. Y. Li, Y. R. Jiang, K. L. Huang, P. Ding, and J. Chen, *J. Alloys Comp.* 466, 451 (2008).
25. H. Y. Zhu, R. Jiang, L. Xiao, and W. Li, *J. Hazard. Mater.* 179, 251 (2010).
26. X. Wen, Y. Cao, X. Qiao, L. Niu, L. Huo, and G. Bai, *Catal. Sci. Technol.* 5, 3281 (2015).
27. W. Li, B. Zhang, X. Li, H. Zhang, and Q. Zhang, *Appl. Catal. A* 459, 65 (2013).
28. M. Zhu and G. Diao, *J. Phys. Chem. C* 115, 24743 (2011).
29. Y. Sun, Z. L. Chen, X. X. Yang, P. Huang, X. P. Zhou, and X. X. Du, *Nanotechnology* 20, 135102 (2009).
30. X. Zhang and L. Jiang, *J. Mater. Chem.* 21, 10653 (2011).

Received: 28 April 2016. Accepted: 13 October 2016.

IP: 185.46.84.218 On: Wed, 06 Jun 2018 07:34:40  
Copyright: American Scientific Publishers  
Delivered by Ingenta